AIP | Physics of Plasmas

Study of electron trapping by a transversely ellipsoidal bubble in the laser wake-field acceleration

Myung-Hoon Cho, Young-Kuk Kim, and Min Sup Hur

Citation: Phys. Plasmas **20**, 093112 (2013); doi: 10.1063/1.4822344
View online: http://dx.doi.org/10.1063/1.4822344
View Table of Contents: http://pop.aip.org/resource/1/PHPAEN/v20/i9
Published by the AIP Publishing LLC.

Additional information on Phys. Plasmas

Journal Homepage: http://pop.aip.org/
Journal Information: http://pop.aip.org/about/about_the_journal
Top downloads: http://pop.aip.org/features/most_downloaded
Information for Authors: http://pop.aip.org/authors

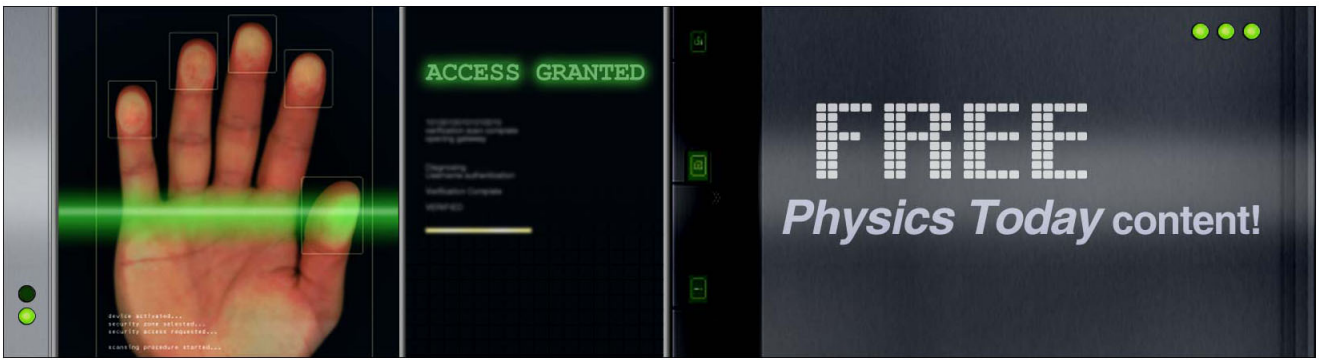

Downloaded 13 Oct 2013 to 114.70.7.203. This article is copyrighted as indicated in the abstract. Reuse of AIP content is subject to the terms at: http://pop.aip.org/about/rights_and_permissions

Study of electron trapping by a transversely ellipsoidal bubble in the laser wake-field acceleration

Myung-Hoon Cho,[1] Young-Kuk Kim,[2] and Min Sup Hur[2,a)]
[1]*School of Natural Science, UNIST, BanYeon-Ri 100, Ulju-gun, Ulsan 689-798, South Korea*
[2]*School of Electrical and Computer Engineering, UNIST, BanYeon-Ri 100, Ulju-gun, Ulsan 689-798, South Korea*

(Received 12 April 2013; accepted 9 September 2013; published online 27 September 2013)

We present electron trapping in an ellipsoidal bubble which is not well explained by the spherical bubble model by [Kostyukov *et al.*, Phys. Rev. Lett. **103**, 175003 (2009)]. The formation of an ellipsoidal bubble, which is elongated transversely, frequently occurs when the spot size of the laser pulse is large compared to the plasma wavelength. First, we introduce the relation between the bubble size and the field slope inside the bubble in longitudinal and transverse directions. Then, we provide an ellipsoidal model of the bubble potential and investigate the electron trapping condition by numerical integration of the equations of motion. We found that the ellipsoidal model gives a significantly less restrictive trapping condition than that of the spherical bubble model. The trapping condition is compared with three-dimensional particle-in-cell simulations and the electron trajectory in test potential simulations. © *2013 AIP Publishing LLC*. [http://dx.doi.org/10.1063/1.4822344]

I. INTRODUCTION

Since Tajima and Dawson first suggested the concept of the plasma-based laser wake-field acceleration and calculated the efficiency of the acceleration comparing it to commercial acceleration methods,[1] many people have investigated that field by theory, computer simulations, and experiments.[2–9] Recently, significant experimental results came out showing quasimonoenergetic dense bunches of relativistic electrons with up to GeV-class energy.[3,4]

The generation of the accelerating wake-field comes from the ponderomotive force of the driving laser pulse. In this mechanism, electrons are first expelled by the ponderomotive force of the laser pulse and then are attracted back to their origins by the electric field induced by the charge separation. When the power of the driving laser pulse exceeds a certain threshold value, i.e., $P > P_c = 30[\mathrm{GW}] \times (\tau[\mathrm{fs}]/\lambda[\mu\mathrm{m}])^2$, this process forms a bubble, which is a spherically shaped electron-free region, having a sheath of higher electron density than that of the background in its rim. The bubble formed in this way propagates with the group velocity of the laser pulse so that $v_0/c \simeq 1 - 1/2\gamma_0^2$ ($\gamma_0 \simeq \omega_0/\omega_p$), where $\omega_p = \sqrt{4\pi n_0 e^2/m}$ is the electron plasma frequency, ω_0 is the laser frequency and v_0, n_0, m, γ_0 are the laser group velocity, the background electron density, the electron mass, and the relativistic factor of the bubble, respectively.

Differently from conventional accelerators, in many experiments and simulations of the electron acceleration in the bubble regime, people do not use a separate beam injector, but instead the electrons are mostly self-injected into the bubble from the background plasma. Depending on the position and duration of such self-injection, most of the important beam parameters like the beam energy, energy spread, emittance, and beam charge are determined. Thus, understanding the self-injection mechanism is the key point in the laser plasma acceleration study. In other contexts, to make a large amount of electrons be self-injected, various additional techniques have been proposed such as two counter propagating laser pulses,[5,15] density transition,[16,17] ionization injection,[18] etc.

From the numerical studies, it has been observed that electrons can be trapped by a large bubble with $R > 4$, where R is the normalized bubble radius to c/ω_p.[2] After that Kostyukov *et al.* derived the trapping condition for a spherical bubble, $\gamma_0 < R/\sqrt{2}$, where γ_0 is the gamma-factor of the bubble's backside.[10] As another mechanism of the electron trapping, it was theoretically suggested that the bubble deformation (usually the bubble's expansion) also traps electrons.[11] Moreover, it was shown in the same reference that subsequent bubble shrinking after the expansion makes a quasi-monoenergetic energy peak in the electron beam. Such a bubble expansion is actually dominant in longitudinal direction, so a longitudinally ellipsoidal bubble theory was introduced.[12]

In this article we describe the electron trapping condition in a transversely elongated ellipsoidal bubble, comparing it with the spherical one. As an overall feature, we show the evolution of the ellipsoidal bubble in Fig. 1, where we traced the longitudinal and transverse bubble size separately, and also the electron trapping by a three dimensional particle-in-cell (PIC) simulation. As can be seen from Fig. 1, the bubble starts with a transversely long ellipsoidal shape $R_y > R_x$ and then it slowly changes into a sphere ($R_x \simeq R_y$). Here, the PIC simulation suggests that the trapping of electrons occurs not only in the spherical regime but also in the ellipsoidal regime, which is not explained by the previous spherical bubble model. To explain this, we generalized the bubble shape in the spherical bubble theory in Ref. 10. First, we introduce the relationship between the ratio of the longitudinal bubble size to the transverse one and the ratio of the

a)Electronic mail: mshur@unist.ac.kr

 © 2013 AIP Publishing LLC

Downloaded 13 Oct 2013 to 114.70.7.203. This article is copyrighted as indicated in the abstract. Reuse of AIP content is subject to the terms at: http://pop.aip.org/about/rights_and_permissions

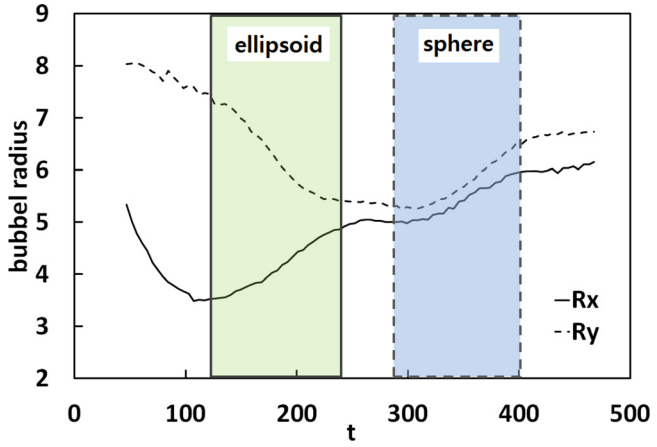

FIG. 1. Electron trapping as the bubble evolves temporally in its longitudinal (R_x) and transverse (R_y) sizes during an entire simulation. The solid box indicates the trapping region of an ellipsoidaly shaped bubble, and the dashed box indicates that of a spherically shaped bubble. The previous spherical bubble model is not sufficient to explain the electron trapping in the ellipsoidal region.

longitudinal field slope inside the bubble to that in the transverse direction. By numerically integrating particle trajectories around such an ellipsoidal bubble potential, we obtained a modified trapping condition for an ellipsoidal bubble. Then, the newly obtained condition was verified by three-dimensional PIC simulations.

This article is organized as follows. In Sec. II, we present the generalized ellipsoidal bubble model. In Sec. III, the modified electron trapping condition is derived with the help of numerical integration of the Hamiltonian equation. In Sec. IV, the newly obtained trapping condition is compared with PIC simulations. Finally a summary is given in Sec. V.

II. MODEL OF THE ELLIPSOIDAL BUBBLE FIELDS

The electromagnetic field in a bubble has a linearly increasing region around the center and a thin sheath region near the bubble's edge. Such a field shape is well approximated by the following function:[10,13]

$$F(r) = k\frac{r}{4}\left(1 - \tanh\frac{r-R}{d}\right), \tag{1}$$

where R is the bubble radius, d the sheath thickness at the bubble boundary, and k the scale factor of the field slope of the bubble. Then, the electromagnetic field inside the bubble becomes $E_x = F(r)$, $E_y = -H_z = F(r)/2$. It is actually observed that Eq. (1) matches well the results from three-dimensional PIC simulations for a long enough simulation period. Integrating Eq. (1) with r, we obtain the bubble potential Φ as follows:

$$\Phi(r) = k\left[\frac{r^2}{8} - \frac{rd}{4}\ln\left(\exp\frac{r-R}{d} + \exp\frac{-(r-R)}{d}\right) + \frac{1}{4}\int_0^r dr'\ln\left(\exp\frac{r'-R}{d} + \exp\frac{-(r'-R)}{d}\right)\right]. \tag{2}$$

Actually the bubble potential is defined as $\Phi = A_x - \phi$ using the gauge of $A_x = -\phi$, where A_x and φ are the x component of a vector potential and a scalar potential, respectively (see Sec. III). By splitting the integration range at $r = R$, the final form of the potential for the region of $r \le R$ becomes

$$\Phi(r) = k\left[\frac{r^2}{4} - \frac{rd}{4}\ln\left(1 + \exp\frac{2(r-R)}{d}\right) - \frac{d^2}{8}Li_2\left(-\exp\frac{2(r-R)}{d}\right) + \frac{d^2}{8}Li_2\left(-\exp\frac{-2R}{d}\right)\right] + \Phi_0, \tag{3}$$

and for the region of $r > R$,

$$\Phi(r) = k\left[\frac{R^2}{4} + \frac{d^2\pi^2}{48} + \frac{d^2}{8}Li_2\left(-\exp\frac{-2R}{d}\right) - \frac{rd}{4}\ln\left(1 + \exp\frac{-2(r-R)}{d}\right) + \frac{d^2}{8}Li_2\left(-\exp\frac{-2(r-R)}{d}\right)\right] + \Phi_0, \tag{4}$$

where $Li_2(x) = \int_x^0 dt\frac{\ln(1-t)}{t}$ is dilogarithm function and $\Phi_0 = 1 - R^2/4$ is the potential at $r = 0$ to make the potential unity at $r = R$. When an ellipsoidal potential is assumed, we use different values for the radii in x and y directions in Eq. (4), being marked by R_x and R_y. Then by assuming that the potential is constant around the bubble rim, we can set the potential as follows:

$$\Phi(R_x + 2d_x; k = k_x) = \Phi(R_y + 2d_y; k = k_y). \tag{5}$$

Here the factor of two in front of the sheath thickness d is just to ensure that the distance is far enough from R. We also use separate values for the field slopes in x and y directions, i.e., k_x and k_y. Then from Eqs. (4) and (5), we obtain the relationship between the field slopes and the bubble sizes in x and y directions as follows:

$$R_y = \sqrt{\frac{k_x}{k_y}}R_x, \tag{6}$$

$$d_y = \sqrt{\frac{k_x}{k_y}}d_x. \tag{7}$$

Equation (6) tells us that the elongation of the ellipsoidal bubble is determined by the ratio of the bubble's field slope in each direction. This relation is well justified in Fig. 2, where it is shown that measured values R_x, R_y, k_x, and k_y from a three-dimensional PIC simulation satisfy well the theoretical relationship, Eq. (6). Here, we notice that the scale factor k_x or k_y is obtained as the ratio of the slope of corresponding electric field component and the maximal value of the field slope (1/2 for E_x and 1/4 for E_y, see Ref. 13). Note that k_x and k_y do not exceed unity.

Equations (3) and (6) along with appropriate $k(\theta)$ (see Eq. (14)) yield the following potential that, in turn, corresponds to elliptical shape of the bubble

Downloaded 13 Oct 2013 to 114.70.7.203. This article is copyrighted as indicated in the abstract. Reuse of AIP content is subject to the terms at: http://pop.aip.org/about/rights_and_permissions

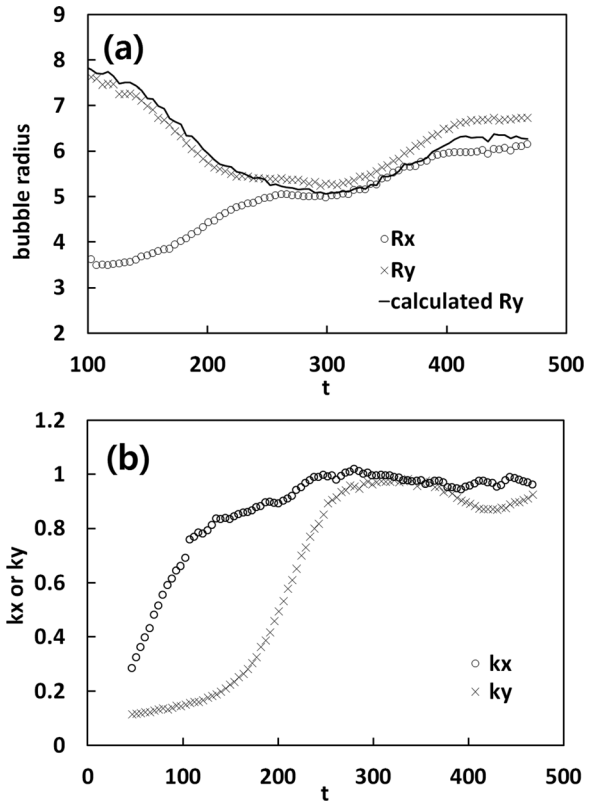

FIG. 2. Evolution of (a) the bubble sizes in longitudinal and transverse directions, and (b) the bubble field slopes in longitudinal and transverse directions. The "calculated R_y" is calculated from $R_x\sqrt{k_x/k_y}$. For this simulation, the laser pulse spot size is $r_L = 1.9\lambda_p$.

$$\Phi = \frac{k_x}{4}x^2 + \frac{k_y}{4}y^2 + \Phi_0. \tag{8}$$

In Eq. (8), we neglected the screening terms that are important only near the bubble rim. Even though this result comes from phenomenological field slopes, the potential shape matched well the PIC simulation result as shown in Figs. 2 and 5.

III. ELECTRON TRAPPING IN AN ELLIPSOIDAL BUBBLE

In this section, we describe the electron trapping condition under the general shape of the bubble described above, i.e., $R_x \neq R_y$. When the group velocity of the driving laser pulse is close to the speed of light so that $\gamma_0^2 = 1/(1 - v_0^2/c^2) \gg 1$, the averaged electron motion in a slowly varying electromagnetic field is determined by the averaged Hamiltonian[14]

$$H = \sqrt{1 + (P + A)^2 + \bar{a}^2} - v_0 P_x - \phi, \tag{9}$$

where P is the canonical momentum of the electron, $\bar{a}$ the vector potential of the laser field, and A and φ the slowly varying vector and scalar potentials, respectively. We change the variables from (x, P_x) to (ξ, P_ξ) using $\xi = x - v_0 t$ and $P_\xi = P_x$. The gauge is chosen as $A_x = -\phi$. Then, by defining the wake potential $\Phi = A_x - \phi$, the Hamiltonian equation of motion is given by[13]

$$\frac{dP_x}{dt} = -v_x\frac{\partial A_x}{\partial \xi} - v_y\frac{\partial A_y}{\partial \xi} + \frac{\partial \phi}{\partial \xi} = -\frac{1}{2}(v_x + 1)\frac{\partial \Phi}{\partial \xi}, \tag{10}$$

$$\frac{dP_y}{dt} = -v_x\frac{\partial A_x}{\partial y} - v_y\frac{\partial A_y}{\partial y} + \frac{\partial \phi}{\partial y} = -\frac{1}{2}(v_x + 1)\frac{\partial \Phi}{\partial y}, \tag{11}$$

$$\frac{d\xi}{dt} = \frac{p_x}{\gamma} - v_0 = v_x - v_0, \tag{12}$$

$$\frac{dy}{dt} = \frac{p_y}{\gamma} = v_y, \tag{13}$$

where p is the kinematic momentum, and $\gamma = \sqrt{1 + p_x^2 + p_y^2}$. Here, we assume that $A_\perp$ and $\bar{a}$ are negligible.

To represent an ellipsoidal potential Φ for Eqs. (10)–(13), we introduce angle dependence of k in Eqs. (3) and (4) such that

$$k(\theta) = k_x \cos^2\theta + k_y \sin^2\theta, \tag{14}$$

where θ is the angle measured from the x-axis. Then we numerically integrated Eqs. (3), (4), and (10)–(13) to calculate the electron trajectories around the bubble potential to examine the trapping or non-trapping of electrons depending on the initial conditions of the bubble. Fig. 3 shows one example of such integration, where it is shown that an electron, which traces a non-trapping route around a spherical

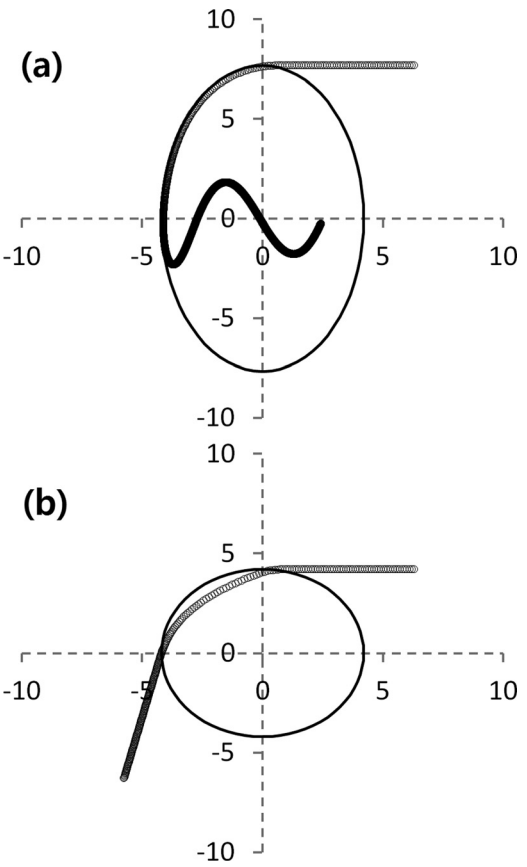

FIG. 3. Trajectories of electrons in (a) the ellipsoidal and (b) the spherical bubble potentials. The gamma factor of the bubble is $\gamma_0 = 4.5$, the bubble radius is $R_x = 4.2$, and the field slopes are (a) $k_x = 1$, $k_y = 0.3$, and (b) $k_x = k_y = 1.0$, for which the condition is non-trapping in the spherical bubble model.

Downloaded 13 Oct 2013 to 114.70.7.203. This article is copyrighted as indicated in the abstract. Reuse of AIP content is subject to the terms at: http://pop.aip.org/about/rights_and_permissions

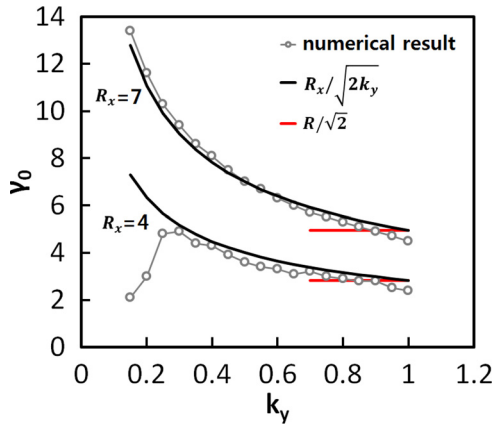

FIG. 4. The numerical calculation of the electron's trapping condition. The red solid line is the condition from the spherical model and the black solid line is a fitting curve with $R_x/\sqrt{2k_y}$ for $R_x = 4$ and $R_x = 7$. Other parameters are $d = 0.05$ and $k_x = 1$.

bubble, can actually be trapped if the bubble is elongated transversely for the same longitudinal bubble conditions such as the bubble speed and the longitudinal bubble size.

To obtain a trapping condition for the ellipsoidal bubble, we performed a series of trajectory calculations numerically, where we tried to determine the maximum value of γ_0 to trap the electron for a given k_y and R_x. Note that as γ_0 decreases, electrons can be trapped more easily. Those numerical results are shown in Fig. 4 for diverse values of R_x and k_y. Then finally the fitting of those numerical results yielded the following condition for electron trapping:

$$\gamma_0 \le \frac{R_x}{\sqrt{2k_y}} = \frac{R_y}{\sqrt{2}}, \tag{15}$$

with parameters $k_x = 1$ and $d = 0.05$ (here we ignore d). Interestingly, the trapping condition is determined by just the transverse radius (R_y). When $R_x < R_y$, even though the focusing field becomes weaker than that of a spherical bubble, i.e., $k_y < 1$, the electrons can still be trapped.

This result could be verified from the test potential calculation with more diverse k_y and R_y as shown in Table I. In this table, note that a k_x is fixed as unity, R_x decreases with decreasing k_y for a given R_y. Table I shows that the trapping condition does not change much as long as R_y is fixed though R_x changes, which is indicated in Eq. (15). This point provides us with an important insight regarding the trapping, since the transversely elongated ellipsoidal bubble appears quite often in the early stage of the bubble formation, which is the regime that the spherical theory does not explain the trapping.

TABLE I. Maximum value of γ_0 obtained from the test potential calculations with fixed $k_x = 1$ and varying k_y and R_y.

	k_y							
R_y	0.3	0.4	0.5	0.6	0.7	0.8	0.9	1.0
5.0	…	…	3.1	3.2	3.2	3.1	3.1	3.1
6.0	…	3.9	3.9	3.9	3.9	3.8	3.8	3.8
7.0	4.5	4.7	4.6	4.6	4.6	4.6	4.6	4.5
8.0	5.5	5.5	5.4	5.4	5.4	5.4	5.4	5.4
9.0	6.2	6.3	6.3	6.3	6.3	6.2	6.2	6.2

Unfortunately we could not find more general relation of k_x, k_y and bubble radius except $k_x = 1$, so we confine the theory for the case of sufficiently large $k_x \sim 1$. However this is a good approximation, since usually the longitudinal field slope reaches the maximum value earlier than the transverse field.

IV. NUMERICAL SIMULATIONS

We carried out three-dimensional PIC simulations to verify the theoretical result in Eq. (15). A detailed explanation and some benchmarks of the PIC code are described in Ref. 19. To generate an ellipsoidal bubble, we used a pulse spot size larger than the plasma wavelength, i.e., $1.9\lambda_p$. It is clearly observed in Fig. 5 that the bubble takes a transversely elongated shape in the early stage. Simulation parameters were as follows; the plasma density was $n_0 = 1.0 \times 10^{19}\,\mathrm{cm}^{-3}$, the

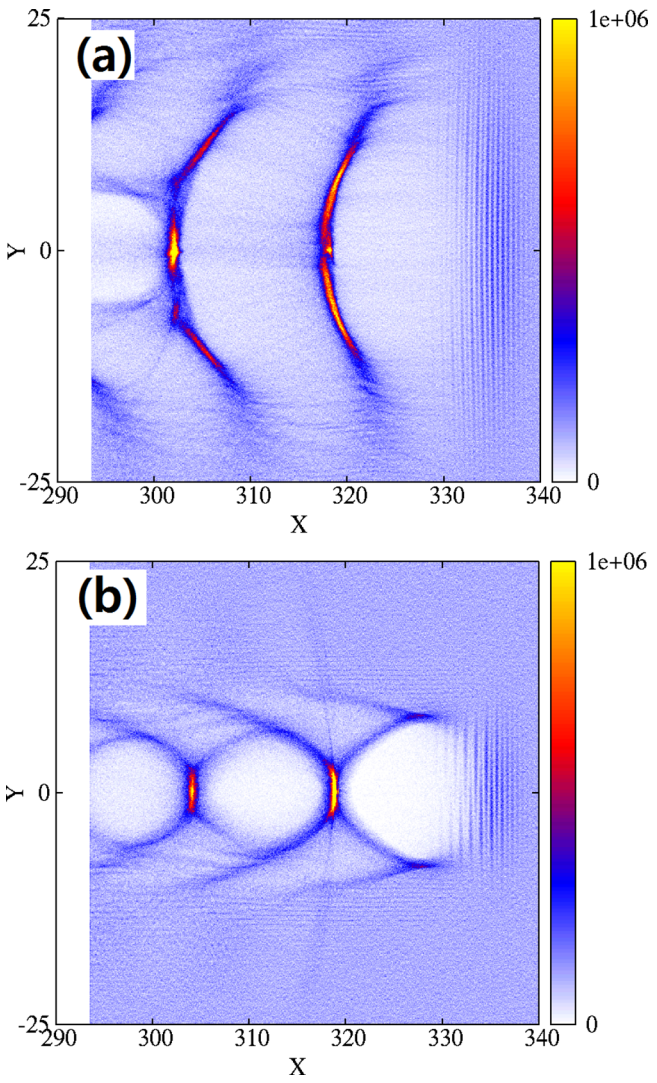

FIG. 5. The distribution of the electron density in the x–z plane from a three-dimensional PIC simulation. The measured laser pulse spot sizes are (a) $r_L = 1.9\lambda_p$, and (b) $r_L = 0.95\lambda_p$, when the laser pulse passes through 340 λ in the plasma.

Downloaded 13 Oct 2013 to 114.70.7.203. This article is copyrighted as indicated in the abstract. Reuse of AIP content is subject to the terms at: http://pop.aip.org/about/rights_and_permissions

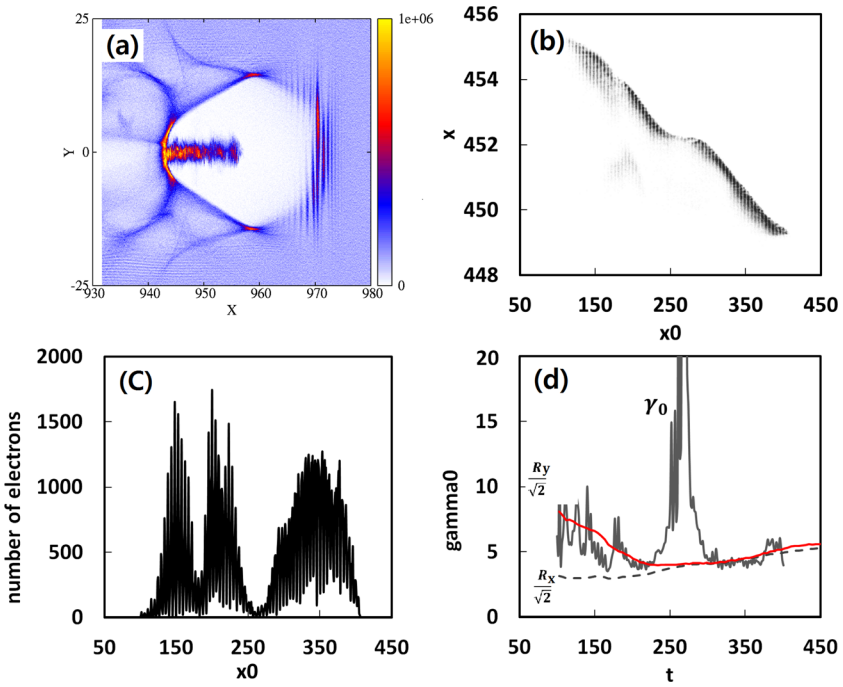

FIG. 6. (a) The distribution of the electron density in the x–z plane from a three-dimensional PIC simulation. (b) The last position x of trapped electrons as a function of x_0. (c) The number of trapped electrons scaled in an x_0 coordinate. (d) The gamma factor of the bubble's backside calculated from Eq. (16) and the measured slope of (b). The grey solid line is the gamma factor of the bubble's backside, the red solid line is $R_y/\sqrt{2}$, and the dashed line is $R_x/\sqrt{2}$ which is the same as the spherical model.

laser pulse was linearly polarized in the y direction with a Gaussian envelope, the wavelength was $\lambda = 0.8\,\mu$m, the normalized vector potential of the laser pulse was $a_0 = 3$, and the pulse duration was 26.6 fs. The simulation stopped when the laser pulse passed the distance of 769 λ inside the plasma.

As the pulse propagates through the plasma, the field slope of bubble starts to increase. When the spot size of the pulse is larger than the plasma wavelength, the transverse field slope is somewhat tardy in growth in comparison with the longitudinal field slope, because the edge field of the laser pulse makes it hard for the electrons to gather around the bubble's sides. In this way, the retarded growth of the transverse field slope forms a transversely elongated ellipsoidal bubble. However as the transverse field slope eventually catches up with the longitudinal field slope, the bubble deforms to the sphere and subsequently the longitudinally elongated bubble.

To compare the theoretical trapping condition (15) with the PIC simulations, the gamma factor γ_0 of the bubble should be calculated. For that purpose, we tracked all the individual particles for an entire simulation period. Trapped particles were initially positioned at the vertical (transverse) edge of a bubble with a low momentum, and they began to be trapped near the backside of the bubble. Then, the gamma factor of the backside of the bubble can be calculated by[10]

$$\gamma_0 \simeq \sqrt{\frac{-1}{2dx/dx_0}}, \tag{16}$$

where x is the last position and x_0 the initial position of the trapped electrons in the trapping process. From the measured slope in x vs. x_0 graphs as in Fig. 6(b), and using Eq. (16), the gamma factor of the bubble's backside can be calculated, which is the grey solid line in Fig. 6(d). The dashed line in Fig. 6(d) indicates the threshold value for the trapping in the spherical bubble model, i.e., $R_x/\sqrt{2}$. If we follows $R_x/\sqrt{2}$, γ_0 is larger than this value during the time t from 100 through 250, so there should be no trapping according to the spherical model, while significant particle trapping was observed as in Fig. 6(c). However that range is actually the ellipsoidal regime, and γ_0 is located at the similar level of or below the modified threshold value $R_y/\sqrt{2}$, so the electron trapping in that temporal range is well explained by the ellipsoidal trapping condition. After the pulse passes through the nontrapping range around $t = 260$, the bubble took the spherical shape and satisfied both the original and the modified trapping conditions.

V. SUMMARY

We have demonstrated by the theory and simulations the self-injection of electrons in the ellipsoidal bubble. Such a transversely elongated bubble appears commonly in the early stage of the pulse propagation, when the pulse spot size is larger than the plasma wavelength. Numerically we found a trapping condition for such ellipsoidal bubbles, where the trapping threshold of γ_0 is described more appropriately by $R_x/\sqrt{2k_y}$ instead of $R_x/\sqrt{2}$ and consequently is just described by $R_y/\sqrt{2}$. We have confirmed this result by numerical integration of test electron trajectories and full three-dimensional PIC simulations. Our result also implies that increasing the spot size of the driving laser pulse enhances early trapping of the electrons. However a more systematic study is required for the optimal bubble and pulse shapes, and the analytic origin of k_x and k_y relating the bubble density and Maxwell's equation, which are actually under progress.

ACKNOWLEDGMENTS

This research was supported by the Basic Science Research Program through the National Research Foundation

Downloaded 13 Oct 2013 to 114.70.7.203. This article is copyrighted as indicated in the abstract. Reuse of AIP content is subject to the terms at: http://pop.aip.org/about/rights_and_permissions

(NRF) of Korea funded by the Ministry of Science, ICT and Future Planning (Grant Nos. NRF-2012-0005931 and NRF-2013R1A1A2006353).

[1]T. Tajima and J. M. Dawson, Phys. Rev. Lett. **43**, 267 (1979).
[2]W. Lu, M. Tzoufras, and C. Joshi, Phys. Rev. ST Accel. Beams **10**, 061301 (2007).
[3]W. P. Leemans, B. Nagler, A. J. Gonsalves, Cs. Toth, K. Nakamura, C. G. R. Geddes, E. Esarey, C. B. Schroeder, and S. M. Hooker, Nat. Phys. **2**, 696 (2006).
[4]N. A. M. Hafz, T. M. Jeong, I. W. Choi, S. K. Lee, K. H. Pae, V. V. Kulagin, J. H. Sung, T. J. Yu, K.-H. Hong, T. Hosokai, J. R. Cary, D.-K. Ko, and J. Lee, Nature Photon. **2**, 571 (2008).
[5]J. Faure, C. Rechatin, A. Norlin, A. Lifschitz, Y. Gilnec, and V. Malka, Nature **444**, 737 (2006).
[6]S. P. D. Mangles, C. D. Murphy, Z. Najmudin, A. G. R. Thomas, J. L. Collier, A. E. Dangor, E. J. Divall, P. S. Foster, J. G. Gallacher, C. J. Hooker, D. A. Jaroszynski, A. J. Langley, W. B. Mori, P. A. Norreys, F. S. Tsung, R. Viskup, B. R. Walton, and K. Krushelnick, Nature **431**, 535 (2004).
[7]C. G. R. Geddes, Cs. Toth, J. van Tilborg, E. Esarey, C. B. Schroeder, D. Bruhwiler, C. Nieter, J. Cary, and W. P. Leemans, Nature **431**, 538 (2004).
[8]J. Faure, Y. Glinec, A. Pukhov, S. Kiselev, S. Gordienko, E. Lefebvre, J.-P. Rousseau, F. Burgy, and V. Malka, Nature **431**, 541 (2004).
[9]A. Pukhov, S. Gordienko, S. Kiselev, and I. Kostyukov, Plasma Phys. Controlled Fusion **46**, B179 (2004).
[10]I. Kostyukov, E. Nerush, A. Pukhov, and V. Seredov, Phys. Rev. Lett. **103**, 175003 (2009).
[11]S. Kalmykov, S. A. Yi, V. Khudik, and G. Shvets, Phys. Rev. Lett. **103**, 135004 (2009).
[12]R. Sadighi-Bonabi and S. H. Rahmatollahpur, Phys. Plasmas **17**, 033105 (2010).
[13]I. Kostyukov, A. Pukhov, and S. Kiselev, Phys. Plasmas **11**, 5256 (2004).
[14]P. Mora and T. M. Antonsen, Jr., Phys. Rev. E **53**, R2068 (1996).
[15]E. Esarey, R. F. Hubbard, W. P. Leemans, A. Ting, and P. Sprangle, Phys. Rev. Lett. **79**, 2682 (1997).
[16]S. Bulanov, N. Naumova, F. Pegoraro, and J. Sakai, Phys. Rev. E **58**, R5257 (1998).
[17]H. Suk, N. Barov, J. B. Rosenzweig, and E. Esarey, Phys. Rev. Lett. **86**, 1011 (2001).
[18]E. Oz, S. Deng, T. Katsouleas, P. Muggli, C. D. Barnes, I. Blumenfeld, F. J. Decker, P. Emma, M. J. Hogan, R. Ischebeck, R. H. Iverson, N. Kirby, P. Krejcik, C. OConnell, R. H. Siemann, D. Walz, D. Auerbach, C. E. Clayton, C. Huang, D. K. Johnson, C. Joshi, W. Lu, K. A. Marsh, W. B. Mori, and M. Zhou, Phys. Rev. Lett. **98**, 084801 (2007).
[19]M. S. Hur and H. Suk, Phys. Plasmas **18**, 033102 (2011).

Downloaded 13 Oct 2013 to 114.70.7.203. This article is copyrighted as indicated in the abstract. Reuse of AIP content is subject to the terms at: http://pop.aip.org/about/rights_and_permissions